Chemical Stability of the Magnetic Oxide EuO directly on Silicon observed by Hard X-ray Photoemission Spectroscopy

C. Caspers,[1,2] M. Müller,[1,2,*] A. X. Gray,[3,4] A. M. Kaiser,[1,3,4] A. Gloskovskii,[5] C. S. Fadley,[3,4] W. Drube,[6] and C. M. Schneider[1,2,7]

[1] *Peter Grünberg Institut (PGI-6), Forschungszentrum Jülich, 52425 Jülich, Germany*
[2] *JARA Jülich-Aachen Research Alliance, Forschungszentrum Jülich, 52425 Jülich, Germany*
[3] *Department of Physics, University of California, Davis, California, USA*
[4] *Materials Sciences Division, Lawrence Berkeley National Laboratory, Berkeley, California, USA*
[5] *Institut für Analytische und Anorganische Chemie, Johannes Gutenberg-Universität, 55128 Mainz, Germany*
[6] *DESY Photon Science, Deutsches Elektronen-Synchrotron, 22603 Hamburg, Germany*
[7] *Fakultät für Physik and Center for Nanointegration Duisburg-Essen (CeNIDE), 47048 Duisburg, Germany*

(Dated: October 6, 2011)

We present a detailed study of the electronic structure and chemical state of high-quality stoichiometric EuO and O-rich Eu_1O_{1+x} thin films grown directly on silicon without any buffer layer using hard x-ray photoemission spectroscopy (HAXPES). We determine the EuO oxidation state from a consistent quantitative peak analysis of $4f$ valence band and $3d$ core-level spectra. The results prove that nearly ideal, stoichiometric and homogeneous EuO thin films can be grown on silicon, with a uniform depth distribution of divalent Eu cations. Furthermore, we identify the chemical stability of the EuO/silicon interface from Si $2p$ core-level photoemission. This work clearly demonstrates the successful integration of high quality EuO thin films directly on silicon, opening up the pathway for the future incorporation of this functional magnetic oxide into silicon-based spintronic devices.

A. Introduction

One major challenge in present-day spintronics research is the efficient electrical injection and detection of spin-polarized electrons in semiconductors (SCs). The most promising strategy is to integrate materials with large spin polarization with a SC, e. g. silicon, thus ultimately permitting the addition of the spin dimension to conventional electronic devices[1]. Owing to its ability to generate almost fully spin-polarized currents[2], the magnetic oxide europium oxide (EuO) has recently been revisited as a material with outstanding potential for spintronics[3–6]. The intriguing coexistence of magnetic and insulating properties—although at low temperatures—makes EuO "spin filter" tunnel barriers highly interesting for solving the long-standing conductivity mismatch problem of spin injection into semiconductors. Besides, the structural compatibility and predicted chemical stability with silicon[7] should allow for a seamless integration of EuO with this mainstay of semiconductors – opening up the perspective to add spin functionality into oxide-based spintronics devices.

Although an exhaustive body of work on the physical properties of EuO bulk single crystals has been compiled since the 1970s[8], high-quality EuO thin films have been little investigated to date. One reason is that EuO is a notoriously difficult system when it comes to preparing stoichiometric and single crystalline thin films. This is due to the instantaneous reactivity of this metastable compound towards higher, non-magnetic oxides, e. g. Eu_2O_3, under excess oxygen atmosphere. Stoichiometric EuO is a SC with a band gap of 1.12 eV[9] and orders ferromagnetically below a Curie temperature of $T_C = 69.3\,K$[10]. Its strong magnetism ($M_S = 7.0\,\mu_B/Eu^{2+}$) arises from the half-filled $4f$ states, which lie ∼2 eV below the Fermi level and constitute the top of the valence bands, as confirmed by a recent low-energy angle-resolved photoemission study[11] and calculations in the LSDA+U approximation[9] (Fig. 2). Despite its tremendous potential for spintronics, the direct stabilization of stoichiometric EuO thin films on silicon without any intermediate buffer layer has not been reported to date, and a detailed picture of the valence state of Eu and the electronic structure depending on the chemical composition is missing. A major reason is the difficulty to probe this highly reactive compound by conventional surface-sensitive photoelectron

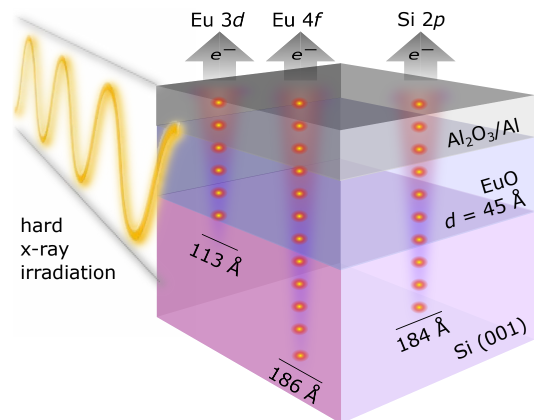

FIG. 1. (color online) Schematics of the bulk-sensitive hard x-ray photoemission (HAXPES) experiment of a Al/EuO/Silicon heterostructure. The calculated information depths for core level and valence band photoelectrons are indicated by arrows for normal emission (0°) geometry.

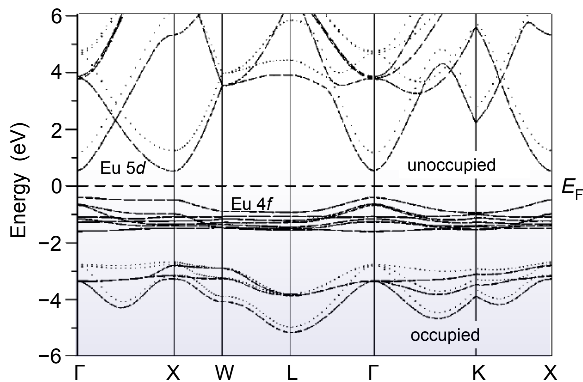

FIG. 2. Band structure of EuO calculated in the LSDA+U approximation. The top of the Eu 4f valence band and the Eu 5d conduction band are indicated. Adapted from Ghosh *et al.*[9]

spectroscopy, given the necessity for a protective capping layer. In response to the need for a bulk-sensitive electronic structure probe, hard x-ray photoelectron spectroscopy (HAXPES) was recently developed as the high-photon energy variant of the well-established photoemission technique, where the photoelectron energy is extended up to several keV[12,13]. The average depth of photoelectron emission is primarily controlled by the inelastic mean free path (IMFP) which is found to increase as about $(E_{\text{kin}})^{3/4}$ for electron energies exceeding about 1 keV, and thus reaches up to typically 10 nm at 10 keV for most systems[14,15]. This not only allows direct access to the bulk electronic structure of buried films, but also enables a depth profiling of their chemical homogeneity, which is not possible with conventional photoelectron spectroscopy (PES) at 1 keV or less.

In this work, we report a detailed study on the valence states and electronic structure of thin EuO films on silicon substrates using HAXPES. In particular, we demonstrate the successful chemical stabilization of stoichiometric EuO thin films grown directly on silicon without any buffer layer. We present hard x-ray photoemission spectroscopy experiments of EuO compounds with different chemical ground states, i. e. stoichiometric EuO and off-stoichiometric oxygen-rich $\text{Eu}_1\text{O}_{1+x}$, and carefully determine the Eu valence state via a quantitative analysis of core-level and valence spectra. We performed depth-sensitive measurements and extracted the Eu valency in the bulk and interface regions, confirming that nearly ideal, homogeneous and stoichiometric thin films of the magnetic oxide EuO can be grown on silicon, without any traces of interfacial silicon dioxide formed at the EuO/Si interface.

B. Experimental Details

The EuO compounds investigated in this study comprised (i) stoichiometric EuO and (ii) oxygen-rich $\text{Eu}_1\text{O}_{1+x}$ films grown by molecular beam epitaxy (MBE) under ultra-high vacuum (UHV) conditions with a base pressure of $p_{\text{base}} \leqslant 1 \times 10^{-10}$ mbar. Si(001) substrates were etched in diluted hydrofluoric (HF) acid in order to remove the native SiO_2 layer and to prepare a H_2-passivated surface. For the EuO synthesis, europium metal (99.99%) was e-beam evaporated with a constant Eu flux density $\varphi_{\text{Eu}} = 2.8 \times 10^{13}$ atoms/cm^2 s. Molecular oxygen gas (99.998%) was simultaneously supplied through a differentially pumped oxygen line equipped with a leak valve, and its pressure was monitored by both an ion gauge and mass spectrometer. A precise control of Eu flux and oxygen partial pressure was maintained during the entire growth process in order to stay within the narrow parameter range where stoichiometric EuO can be stabilized. Taking advantage of the distillation condition bewaring excess Eu during the oxide growth[16,17], we fabricated 45 Å thick EuO films with different stoichiometries (i) and (ii) using a constant O_2 partial pressure in the range $p_{\text{ox}}^{\text{partial}} = 2\text{–}4 \times 10^{-9}$ mbar at an elevated substrate temperature $T_{\text{S}} = 350\,°\text{C}$. This yielded polycrystalline EuO as verified by x-ray diffraction. Details of the structural characterization will be reported elsewhere. Finally, the EuO samples were capped by a 40 Å thick Al film to prevent oxidation in air. In order to account for the high reactivity of EuO, high vacuum conditions were persistently maintained during sample storage and transport.

HAXPES experiments were performed at the undulator beamline P09 at PETRA III (DESY, Hamburg) using a UHV chamber equipped with a multichannel hemispherical electron energy analyzer (SPECS Phoibos 225 HV). The excitation energy was set to 4.2 keV, resulting in kinetic energies larger than 3 keV for the Eu 3d photoemission lines which is sufficient to obtain the required depth sensitivity. It is also noted that at these electron energies there are no interferences with Auger cascades from the Al (cap layer) and Si (substrate) K-shell as well as from the Eu M-shell. The total energy resolution at this photon energy was 500 meV using a Si(111) monochromator, and all spectra were recorded at room temperature. The binding energy scale was calibrated to the metallic Fermi edge of an Au foil in electrical contact with the sample, while the samples were grounded and no effects of charging have been observed during the measurements. In the geometry chosen for this experiment, the electron analyzer accepts emitted electrons at 45° relative to the incoming photons, and angle-dependent spectra in the horizontal plane were measured by rotating the sample around an axis vertical to the plane of x-ray incidence and photoelectron acceptance, in order to take advantage of angle-resolved PES (ARPES) for varying depth sensitivity. In ARPES, the mean depth of electron emission varies as $\cos(\alpha)$, with α being the off-normal emission angle[18]. Shirley-type backgrounds were subtracted from the raw spectra to account for inelastic scattering of the photoelectrons.

In the following, we refer to the effective photoelectron

information depth D_z as the depth z down to which 90% of the photoelectrons are emitted. In a consistent calculation, we determined D_z for our heterostructure ($Al_2O_3^{2\,nm}/Al^{2\,nm}/EuO^{4.5\,nm}/Si$) by taking into account the material-specific electron escape depth λ_{eff} and an exponential damping factor $\exp(-z/\lambda_{\text{eff}})$ in each layer[15,19]. For $4f$ photoelectrons emitted in normal emission (ne) and 43° off-normal emission (oe) geometry, respectively, we estimate $D_{4f}^{ne} = 24\,\text{nm}$ and $D_{4f}^{oe} = 17\,\text{nm}$, whereas the Eu $3d$ photoelectrons yield the information depths $D_{3d}^{ne} = 14.6\,\text{nm}$ and $D_{4f}^{oe} = 10.3\,\text{nm}$.

C. Magnetic properties of EuO/Silicon

With the aim to corroborate the electronic structure analysis by magnetization (M) measurements, in a first step we investigated the magnetic properties of both types of EuO/Si heterostructures (i) and (ii) using a Quantum Design superconducting interference device (SQUID) magnetometer.

Fig. 3 shows the $M(T)$ and $M(H)$ characteristics for (i) stoichiometric EuO and (ii) oxygen-rich Eu_1O_{1+x} thin films on silicon. In stoichiometric EuO, $M(T)$ roughly follows a Brillouin function with spin angular momentum $S = 7/2$[8]. We determined a strong magnetic saturation moment of $M_S = 6.7\,\mu_B$, which is just slightly reduced from the bulk value of $7\,\mu_B$ per Eu^{2+} expected for a $4f^7$ system. Likewise, the normalized $M(H)$ characteristics taken at 2 K (see inset of Fig. 3) displays a clear square-like ferromagnetic hysteresis with a coercive field of $H_c \approx 100$ Oe, indicative of the high magnetic quality of the (i) stoichiometric EuO/Si(001) heterostructure.

For oxygen-rich EuO, in contrast, the $M(T)$ curve in Fig. 3 is almost completely suppressed. Consequently, a strongly reduced magnetic saturation moment $M_S = 1.5\,\mu_B$ is determined at 2 K, which is due to the large fraction of antiferromagnetic Eu^{3+} cations in Eu_2O_3 that instantaneously forms under oxygen excess. This dominating antiferromagnetic behavior is also reflected in the $M(H)$ curve of oxygen-rich EuO in the inset of Fig. 3, in which a hysteretic behavior is hardly identified. Remarkably, the precisely controlled oxygen partial pressure supplied during EuO synthesis differs by only 2×10^{-9} mbar for EuO/Si samples (i) and (ii), this in thus an extremely important parameter in determining the quality of the EuO films.

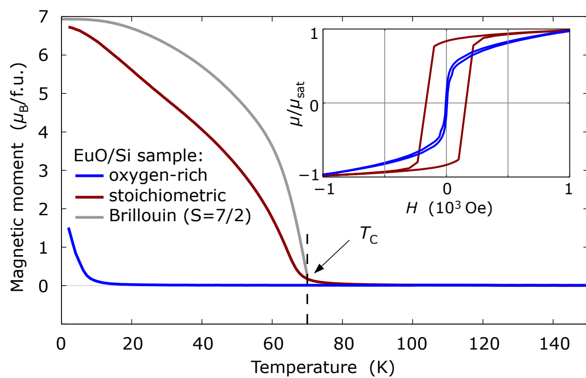

FIG. 3. (color online) Temperature-dependent magnetization of (i) stoichiometric EuO and (ii) O-rich Eu_1O_{1+x} thin films on Si(001). The inset shows the normalized magnetization μ/μ_{sat} versus applied field H for sample types (i) and (ii)

D. HAXPES: Eu 4f valence bands

The most direct information on the oxidation state of Eu compounds is obtained from the $4f$ photoemission. Due to the highly localized character of the $4f$ valence band with a dispersion of up to only 0.3 eV[9,20], hybridization with other ligand states is weak and photoemission from the deeper bound oxygen $2p$ valence band becomes well distinguishable. In contrast to core-level spectroscopy, also final state screening effects of the $4f$ photo-hole should play a less important role. Depending on the Eu_1O_{1+x} stoichiometry, Eu cations will be either in a divalent Eu^{2+} initial state with half-filled $4d^{10}\,4f^7$ shell and a ferromagnetic moment of $7.0\,\mu_B$, or exist as trivalent Eu^{3+} occupying a $4d^{10}\,4f^6$ level, which is chemically shifted towards higher binding energies by reduced Coulomb repulsion and couples antiferromagnetically; this $4f^6$ configuration will exhibit more complex final-state multiplet effects that have been studied elsewhere[21]. Fig. 4 (a) and (c) depict $4f$ photoemission of both EuO compounds (i) and (ii), respectively, recorded in normal emission (ne) geometry. A pronounced peak centered at 1.8 eV below E_F is observed in both spectra, which can be clearly identified as due to electron emission from the divalent Eu^{2+} initial state with $4f^7 \to 4f^6$ final state configuration. The peak shape agrees well with the calculated divalent Euf $4f$ multiplet depicted in Fig. 4 (e)[22]. In Fig. 4 (a), a broad spectral contribution centered at ~4.8 eV below E_F is assigned to the emission from O $2p$ states, which originate from both EuO and Al_2O_3. The absence of a second multiplet in the higher binding energy region in Fig. 4 (a) indicates, that the Eu cations in compound (i) are mainly of divalent valency.

In Fig. 4 (c), in contrast, the $4f$ spectrum of the EuO compound (ii) shows a large additional multiplet structure in the binding region from 5–13 eV below E_F, which corresponds to the $4f^6 \to 4f^5$ final state multiplet of trivalent Eu^{3+}. This broad final state structure is observed in accordance with previous experimental works on Eu^{3+} compounds[23–26] and calculated multiplet lines[21,27] (Fig. 4 (e)). The contribution of the overlapping O $2p$ peak has significantly increased. From the presence of both $4f^6$ and $4f^5$ final state multiplets, we anticipate, that the initial state valency of Eu in compound (ii) is of mixed divalent and trivalent nature.

In order to quantify the initial state valency of both EuO compounds (i) and (ii), we determine the spectral contributions of divalent ($n = 7$) and trivalent

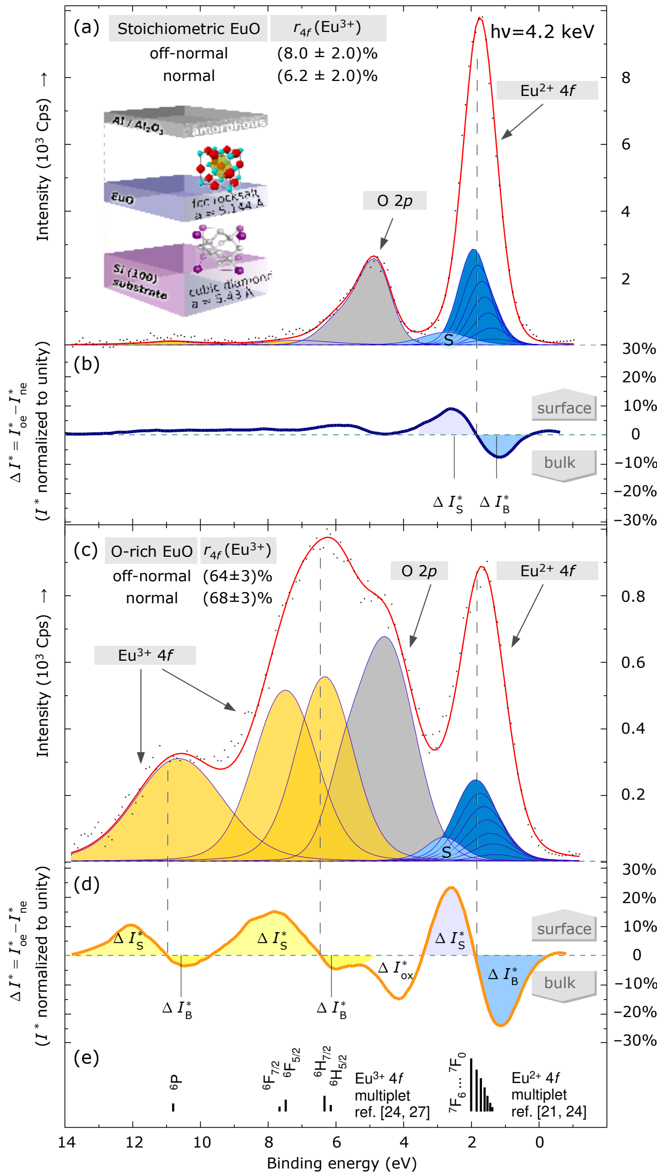

FIG. 4. (color online) $4f$ photoemission spectra of (a) stoichiometric EuO and (c) O-rich EuO on Si recorded at $h\nu = 4.2\,\text{keV}$ in normal emission geometry. The spectra (dots) are fitted well by Gaussian-Lorentzian lines (solid curves) related to emission from divalent and trivalent Eu cations. Panels (b) and (d) show the difference curves of normal and off-normal emission for the normalized $4f$ spectra

$(n = 6)$ Eu cations from the respective $4f^{n-1}$ peak intensities. However, the EuO surface electronic structure may significantly differ from that of bulk EuO, due to changes in local atomic geometry or coordination in direct proximity to the Al_2O_3 capping layer. Consequently, a photoemission peak may be composed of surface-like and bulk contributions, shifted in binding energy E_B by $\delta_S = E_B^{\text{surface}} - E_B^{\text{bulk}}$. To discriminate between bulk and surface-like emission, one has to substantially vary the depth sensitivity of the HAXPES experiment. This has been achieved by recording spectra in normal emission (ne) and 43° off-normal emission (oe) geometry. From our calculated energy and angle-dependent information depths D_{4f} of photoelectrons[15,19], an enhanced surface sensitivity of 30% for $4f$ photoemission in *oe* geometry compared to the bulk-sensitive *ne* geometry can be expected.

Depth-dependent information can be extracted from Fig. 4 (b) and (d), which display the difference intensity curves of the normalized and background-corrected $4f$ spectra recorded in *oe* and *ne* geometry, $\Delta I^*_{4f} = I^*_{oe} - I^*_{ne}$. From these plots, modifications in spectral weight of the Eu $4f$ final states originating from the changed surface sensitivity between *oe* and *ne* geometry are illustrated. In particular, $\Delta I^* < 0$ (> 0) refers to contributions from bulk (I^*_B) (surface (I^*_S)) emission. In Fig. 4 (b) and (d), for both EuO compounds (i) and (ii) we observe a redistribution in peak intensity within the divalent $Eu^{2+}\,4f^6$ final state from the lower binding energy side $(-\Delta I^*_B)$ towards the higher binding energy side $(+\Delta I^*_S)$. This result suggests, that the $4f^6$ final state multiplet of both EuO compounds is composed of a bulk component B, located at a binding energy of $E_B \cong 1.6\,\text{eV}$, and a surface component S shifted towards higher binding energy. The $Eu^{2+}\,4f$ binding energy shifts for the EuO compounds (i) and (ii) amount to $\delta_S^{(i)} = 1.2\,\text{eV}$ and $\delta_S^{(ii)} = 1.3\,\text{eV}$, respectively. A quantitative analysis of the $Eu^{3+}\,4f$ interface shift is impeded by the overlap with the O $2p$ states.

Proceeding with the quantitative analysis of the $4f$ photoemission spectra in Fig. 4 (a) and (c), the line shapes of the $4f^{n-1}$ multiplets were fitted using convoluted Gaussian-Lorentzian curves. Three tunable parameters were employed for least-squares fitting, namely the energy separation between the divalent and trivalent Eu contributions, their intensity ratio and the spectral width (FWHM). For Eu^{2+} peak fitting, a multiplet fine structure was employed in accordance with theoretical calculations in Ref. [28]. The result of the fitting procedure is summarized in Tab. I and shown by the solid curves in Fig. 4 (a) and (c), which match the experimental data points very well. From the integrated spectral intensities A of the Eu^{2+} and Eu^{3+} components, we derive the relative fraction of trivalent Eu as $r^{Eu^{3+}} = A^{Eu^{3+}} / (A^{Eu^{2+}} + A^{Eu^{3+}})$. For the EuO compound (i), we determine a mainly integral divalent chemical state of the Eu cations (trivalent contribution $r_{4f}^{Eu^{3+}} \approx 6\%$). For the EuO compound (ii), in contrast, a mixed initial valency with a trivalent contribution of $r_{4f}^{Eu^{3+}} \approx 68\%$ is derived. Hence, we can refer to the EuO compounds as (i) *stoichiometric* EuO and (ii) *oxygen-rich* Eu_1O_{1+x}. The Eu^{3+} spectral fit neglects Al $3s$ and Al^{3+} $3s$ contributions from the cap layer in this energy region[29], which may lead to a slight over-estimation of $r_{4f}^{Eu^{3+}}$. Our quantitative Eu $4f$ photoemission analysis is corroborated by the magnetic measurements (see Fig. 3): The magnetic saturation moment M_S for the stoichiometric thin EuO

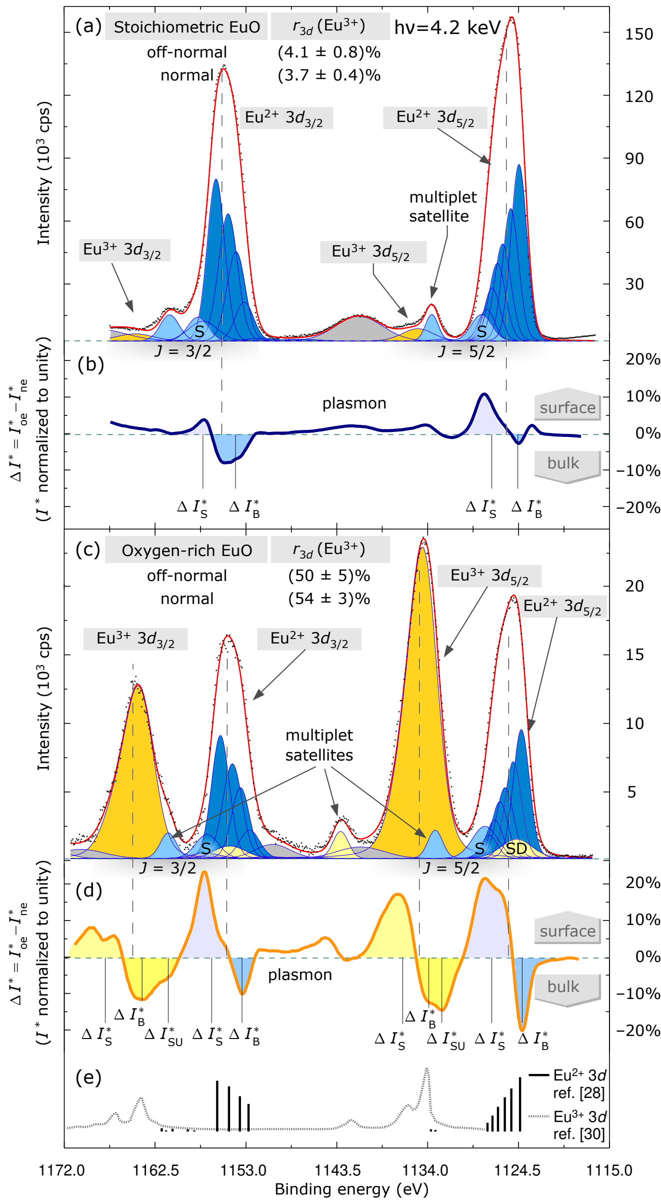

FIG. 5. (color online) $3d$ core-level photoemission spectra for (a) stoichiometric EuO and (c) O-rich Eu_1O_{1+x} films on Si measured in normal emission and at $h\nu = 4.2$ keV. (b) and (d): Difference intensity curves ΔI^* for $3d$ normal and off-normal emission

film (i) was determined as $M_S = 6.7\,\mu_B$, reduced by only about 5% compared to the bulk value of $7\,\mu_B$. For the O-rich EuO sample (ii), a significantly reduced $M_S = 1.5\,\mu_B$ was measured due to the large fraction of antiferromagnetic Eu^{3+} cations.

E. HAXPES: Eu 3d core-levels

In order to check for the consistency of our quantitative analysis of the Eu initial state valency, we proceed by investigating the more deeply bound Eu $3d$ core-levels, which are well accessible by HAXPES. We note, that analyzing the $3d$ core-level spectra has a significant advantage for the determination of the initial state Eu valency compared e.g. to the $4d$ core-levels, because the $3d$ states show a much weaker multiplet splitting and larger photoexcitation cross section.

Fig. 5 (a) and (c) display the Eu $3d$ photoemission spectra for EuO compounds (i) and (ii), recorded in ne geometry. The spectra consist of two main groups, the $3d_{5/2}$ and $3d_{3/2}$ structures, which are clearly separated due to a large spin-orbit splitting of 29.2 eV, in excellent agreement with previous works[26]. The broad structure in the center is assigned to plasmon excitations caused by fast $3d$ photoelectrons passing the Al top layer[22], as it occurs at the correct value of energy loss (16 eV) from the $3d_{5/2}$ peak (and $3d_{3/2}$ peak, which is out of the diagram range).

For (i) stoichiometric EuO, one main peak is observable in the Eu $3d_{5/2}$ and $3d_{3/2}$ groups in Fig. 5 (a). The observed asymmetry in the line shapes is perfectly consistent with theoretical calculations of the divalent Eu $3d$ multiplet, as depicted for comparison in Fig. 5 (e)[28]. We identify a satellite peak in the high binding energy region of the Eu $3d_{5/2}$ and $3d_{3/2}$ multiplet, respectively, which is separated by 7.8 eV (6.3 eV) from the $3d_{5/2}$ ($3d_{3/2}$) main peak. These main peak / satellite doublets are assigned to the divalent Eu^{2+} multiplet of the $3d^9\,4f^7$ final state. Both energy splitting and intensity ratios compare well with previous reports of calculated and measured multiplet spectra of divalent Eu compounds[28,30].

Moving to the oxygen-rich EuO compound (ii) in Fig. 5 (c), we observe prominent double peak structures in the $3d_{5/2}$ ($3d_{3/2}$) regions, which are separated by about 10.45 eV (10.90 eV). We assign these features to divalent Eu^{2+} ($3d^9\,4f^7$ final state) and trivalent Eu^{3+} ($3d^9\,4f^6$ final state) spectral contributions. The Eu^{3+} $3d$ multiplet consists of a doublet, in which the satellite peak appears at 6.9 eV higher binding energy below the $3d_{5/2}$ main peak. The energy positions of the Eu^{2+} and Eu^{3+} $3d$ multiplet structures agree very well with previous experiments[25,31,32] and theoretical calculations, as shown in Fig. 5 e[28,30].

For a depth-sensitive analysis of the $3d$ core-levels, the energy and angle-dependent information depths are calculated as $D^{ne}_{3d} \approx 146$ Å and $D^{oe}_{3d} \approx 103$ Å, indicating an increase in surface sensitivity of 39% for both emission geometries compared to $4f$ photoemission. Fig. 5 (b) and (d) show the $3d$ difference intensity curves $\Delta I^*_{3d} = I^*_{oe} - I^*_{ne}$ for both EuO compounds (i) and (ii). In contrast to the $4f$ spectra, however, an imbalance in intensity transfer between bulk and surface photoemission contributions is apparent, with $|-\Delta I^*_B| \leqslant |+\Delta I^*_S|$. This eminent spectral intensity from more surface-like states is most likely explained by the significantly enhanced surface sensitivity of the $3d$ photoelectrons.

For the quantitative analysis of the Eu $3d$ core-levels, we performed the curve fitting of the Eu^{2+} $3d$ multiplet fine structure in accordance with Ref. [28] using convoluted

Gaussian-Lorentzian lines with consistent intensity ratios, peak widths and energy differences. For the fitting of the Eu^{3+} $3d$ line shapes, we used single Gaussian-Lorentzian peaks, respectively, since the explicit fine structure of the trivalent Eu $3d$ multiplet is unknown. Moreover, we assumed contributions from a well-known Eu^{3+} $3d$ final state effect[31], labelled as SD and Δ^*_{SD} in Fig. 5 (c) and (d). For Eu^{3+} cations, a shake-down satellite (SD) may transfer intensity on the low binding energy side of the main photoemission peak. Its origin is the electrostatic interaction between the $3d$ core hole and the unoccupied $4f$ level[25], described by the Anderson impurity model[33]. Furthermore, for both Eu^{2+} $3d$ and Eu^{3+} $3d$ main peaks, a small surface spectral contribution S is incorporated on the higher binding energy side to account for the increased surface sensitivity of $3d$ photoemission. The result of the fitting procedure, shown by the solid lines in Fig. 5 (a) and (c), shows a very good agreement with the experimental data.

We determined the relative fraction of Eu^{3+} cations as $r_{3d}^{\mathrm{Eu}^{3+}} \approx 0.04$ for EuO compound (i) and $r_{3d}^{\mathrm{Eu}^{3+}} \approx 0.54$ for sample (ii). This result is in good agreement with the quantitative analysis of the $4f$ valence states, as summarized in Table I. For EuO compound (i), we determine a just slightly reduced fraction of Eu^{3+} cations from the $3d$ core-levels (4%) compared to the $4f$ valence states (6%). This result reveals the excellent chemical quality of the MBE-deposited EuO thin films, with a homogeneous depth distribution of Eu cations.

For (ii) oxygen-rich EuO, we extract an about 15% reduced fraction of Eu^{3+} cations from the more interface-sensitive $3d$ compared to the $4f$ emission, indicating a small accumulation of Eu^{2+} cations at the Al interface. The feature is consistently observed for both emission geometries in the Eu $4f$ and Eu $3d$ peak analysis. Given the larger Gibbs free energy of formation G°_{f} for α-Al_2O_3 (−1582 kJ/mol) compared to Eu_2O_3 (−1559 kJ/mol)[34], excess oxygen originating from the oxygen-rich EuO film is preferably bound in α-Al_2O_3 at the interface, reducing the fraction of Eu^{3+}. The counteracting chemical reaction, i. e. the reduction of EuO (−1680 kJ/mol) with metallic Al into Al_2O_3 (−1582 kJ/mol) and metallic Eu, is thermodynamically unfavored.

F. HAXPES: Si 2p core levels

Finally, we investigate the chemical state of the EuO/silicon interface, which is the relevant interface for applications in spin-dependent transport devices. Photoemission from the Si $2p$ core level was recorded in ne and oe geometry. In this way, the information depth D_z of the Si $2p$ photoelectrons is varied between ∼184 Å (ne) and ∼132 Å (oe), respectively, which allows one to distinguish spectral contributions from bulk and interface-like electronic states of the buried Si substrate.

For (i) stoichiometric EuO/Si(100), we observe a well-resolved Si $2p$ doublet structure in Fig. 6 (a), which is indicative for an integral Si^0 valency both in the bulk and interface regions of the substrate. The spectrum can be decomposed into the Si $2p_{1/2}$ and Si $2p_{3/2}$ lines, with a peak intensity ratio of 0.5 and separated by a spin-orbit splitting of 0.6 eV, in perfect agreement with literature[35]. Photoemission contributions from other Si $2p$ valences are absent in the spectrum.

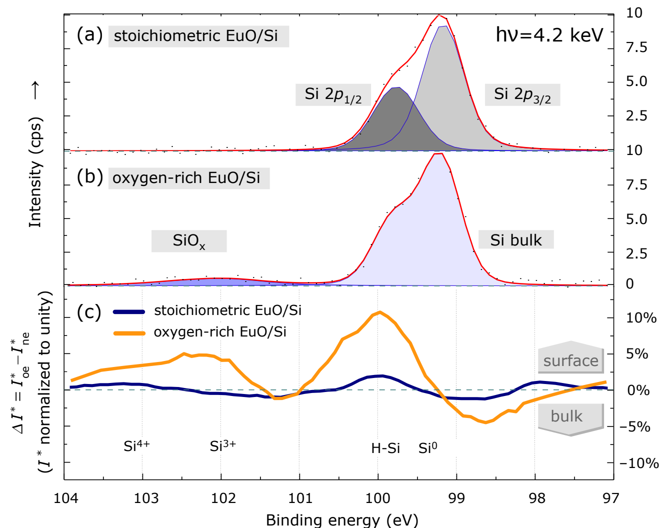

FIG. 6. (color online) Silicon $2p$ core-level photoemission spectra for (a) stoichiometric EuO and (b) O-rich Eu_1O_{1+x} films on Si, both measured in normal emission at $h\nu$ = 4.2 keV. (c) Difference intensity curves of the normalized Si $2p$ core level spectra recorded in ne and oe geometry

In (ii) oxygen-rich EuO, in contrast, besides the sharp Si^0 $2p$ peak, a small, broad feature can be observed on the higher binding energy side in Fig. 6 (b), which is chemically shifted by ∼ 3.1 eV. This finding suggests the formation of silicon oxide SiO_x, however, in case of a complete SiO_2 oxidation the full chemical shift of the corresponding Si^{4+} $2p$ state would amount ∼ 4 eV[14]. We therefore assume that also intermediate oxidation states Si^{3+} exist in addition to Si^{4+} contributions[35].

Analyzing the difference intensity curves $\Delta I^* = I^*_{oe} - I^*_{ne}$ of the normalized Si $2p$ spectra recorded in ne and oe geometry gives further insight into the differences in the local electronic structure between Si bulk and at the EuO/silicon interface. In Fig. 6 (c), we observe a nearly featureless ΔI^* curve for (i) stoichiometric EuO. This result reveals, that no silicon dioxide is formed at the EuO/Si interface, if the Si substrate is covered with (i) stoichiometric EuO. This experimentally observed chemical stability of the EuO/Silicon interface is also corroborated by thermodynamic calculations[7].

For (ii) oxygen-rich EuO, however, a pronounced redistribution of Si $2p$ spectral weight $|-\Delta I^*_{\mathrm{B}}| \leq |+\Delta I^*_{\mathrm{I}}|$ is observed in Fig. 6 (c) in the Si^0 and Si^{3+}/Si^{4+} regions, respectively. We assume the following mechanisms to happen at the O-rich EuO interface: On the one hand, the enhanced Si^{3+}/Si^{4+} contributions underline, that sil-

TABLE I. Binding energies E_B, surface shifts δ_S, and Eu^{3+} valency ratios $r^{\mathrm{Eu}^{3+}}$ for (*i*) EuO and (*ii*) $\mathrm{Eu_1O_{1+x}}$.

Eu 4f	E_B (Eu^{2+})			δ_S (Eu^{2+})		E_B (Eu^{3+})			δ_S (Eu^{3+})		$r_{4f}^{\mathrm{Eu}^{3+}}$	
EuO	1.8 eV			1.2 eV		7.0–11.1 eV			[a]		7.4 ± 1.2%	
$\mathrm{Eu_1O_{1+x}}$	1.64 eV			1.3 eV		7.0–11.1 eV			1.6 eV		66 ± 2%	
Eu 3d	E_B (Eu^{2+})			δ_S (Eu^{2+})		E_B (Eu^{3+})			δ_S (Eu^{3+})		$r_{3d}^{\mathrm{Eu}^{3+}}$	
j =	5/2	3/2	SO	5/2	3/2	5/2	3/2	SO	5/2	3/2	5/2	3/2
EuO	1124.9 eV	1154.1 eV	29.2 eV	1.4 eV	1.4 eV	1134.7 eV	1164.4 eV	29.7 eV	[a]		4.1%	3.2%
$\mathrm{Eu_1O_{1+x}}$	1125.0 eV	1154.3 eV	29.3 eV	2.1 eV	2.9 eV	1134.8 eV	1164.5 eV	29.7 eV	2.0 eV	2.4 eV	59%	49%

[a] This result cannot be determined for the particular peaks due to their low intensity.

icon oxide is mainly formed at the oxygen-rich EuO/Si interface. Due to the low amount of excess oxygen during synthesis of oxygen-rich EuO, also spectral contributions from the lower Si^{3+} oxidation state are observed. On the other hand, we assign the enhanced spectral contribution on the lower Si^{0} $2p$ binding energy side to interfacial Si-H bonds—caused by HF-etching of the Si substrate prior to deposition—which are in the order of $< 1\,\mathrm{eV}$[35]. Further HAXPES studies are underway to monitor the chemical state of the EuO/silicon interface depending on the preparation conditions of $\mathrm{Eu_1O_{1+x}}$ in more detail.

From the above results we conclude, that the chemical state of the EuO/Si(001) interface directly correlates with the specific EuO growth conditions at elevated substrate temperatures. In particular, any oxygen excess during EuO synthesis not only leads to the formation of antiferromagnetic $\mathrm{Eu_2O_3}$, but also promotes an oxidation of the EuO/Si interface. Only if the Eu distillation process and specific range of oxygen supply is precisely matched during synthesis, high quality EuO thin films can be grown directly on silicon without interface oxidation, and can be ultimately integrated on silicon as efficient "spin filter" tunnel injector and collector contacts.

G. Summary

In summary, we have presented a detailed study of the valence state and electronic structure of high-quality EuO and oxygen-rich $\mathrm{Eu_1O_{1+x}}$ thin films grown directly on silicon without buffer layer using HAXPES. We extracted the initial state EuO valency from a quantitative peak analysis of $4f$ valence and $3d$ core-level photoemission spectroscopy, and positively identified a mainly integral divalent Eu valency in stoichiometric EuO thin films. We find a homogenous distribution of Eu cations in the bulk and surface regions, emphasizing the high quality of the MBE-deposited EuO thin films. A chemically stable EuO/silicon interface is identified from Si $2p$ core-level spectroscopy, which is the relevant transport interface for spintronics applications. Our study explicitly demonstrates the successful stabilization of stoichiometric EuO thin films directly on silicon, and points encouragingly towards the future integration of this functional magnetic oxide into silicon-based spintronic devices.

H. Acknowledgements

M.M. acknowledges financial support by DFG under grant MU 3160/1-1. This work was supported by BMBF under contracts 813405-8 WW3 and 05K10CHB. C.S.F. acknowledges salary and travel by the Director, Office of Science, Office of Basic Energy Sciences, Materials Sciences and Engineering Division, of the U.S. Department of Energy under contract No. DE-AC02-05CH11231.

* mart.mueller@fz-juelich.de

1. S. D. Bader and S. S. P. Parkin, Annu. Rev. Condens. Matt., **1**, 71 (2010).
2. G.-X. Miao, M. Münzenberg, and J. S. Moodera, Rep. Prog. Phys., **74**, 036501 (2011).
3. A. Schmehl, V. Vaithyanathan, A. Herrnberger, S. Thiel, C. Richter, M. Liberati, T. Heeg, M. Röckerath, L. F. Kourkoutis, S. Mühlbauer, P. Böni, D. A. Muller, Y. Barash, J. Schubert, Y. Idzerda, J. Mannhart, and D. G. Schlom, Nat. Mater., **6**, 882 (2007).
4. M. Müller, G.-X. Miao, and J. S. Moodera, Europhys. Lett., **88**, 47006 (2009).
5. G.-X. Miao, M. Müller, and J. S. Moodera, Phys. Rev. Lett., **102**, 076601 (2009).
6. M. Müller, M. Luysberg, and C. M. Schneider, Appl. Phys. Lett., **98**, 142503 (2011).
7. K. J. Hubbard and D. G. Schlom, J. Mater. Res., **11**, 2757 (1996).
8. A. Mauger and C. Godart, Phys. Rep., **141**, 51 (1986).
9. D. B. Ghosh, M. De, and S. K. De, Phys. Rev. B, **70**, 115211 (2004).
10. A. Kornblit and G. Ahlers, Phys. Rev. B, **11**, 2678 (1975).
11. H. Miyazaki, T. Ito, S. Ota, H. Im, S. Yagi, M. Kato, K. Soda, and S.-I. Kimura, Physica B, **403**, 917 (2008).
12. K. Kobayashi, Nucl. Instr. Meth. A, **601**, 32 (2009).
13. C. S. Fadley, J. Electron Spectrosc., **178**, 2 (2010).
14. W. Drube, Nucl. Instr. Meth. A, **547**, 87 (2005).

[15] S. Tanuma, C. J. Powell, and D. R. Penn, Surf. Interf. Analysis, **43**, 689 (2011).
[16] P. G. Steeneken, L. H. Tjeng, I. Elfimov, G. A. Sawatzky, G. Ghiringhelli, N. B. Brookes, and D.-J. Huang, Phys. Rev. Lett., **88**, 047201 (2002).
[17] R. Sutarto, S. G. Altendorf, B. Coloru, M. Moretti Sala, T. Haupricht, C. F. Chang, Z. Hu, C. Schüßler-Langeheine, N. Hollmann, H. Kierspel, H. H. Hsieh, H.-J. Lin, C. T. Chen, and L. H. Tjeng, Phys. Rev. B, **79**, 205318 (2009).
[18] C. S. Fadley, Surf. Interf. Anal., **40**, 1579 (2008).
[19] C. J. Powell, A. Jablonski, I. S. Tilinin, S. Tanuma, and D. R. Penn, J. Electron Spectrosc., **98**–**99**, 1 (1999).
[20] H. Miyazaki, T. Ito, H. J. Im, S. Yagi, M. Kato, K. Soda, and S. Kimura, Phys. Rev. Lett., **102**, 227203 (2009).
[21] J. K. Lang, Y. Baer, and P. A. Cox, Journal of Physics F: Metal Physics, **11**, 121 (1981).
[22] W.-D. Schneider, C. Laubschat, I. Nowik, and G. Kaindl, Phys. Rev. B, **24**, 5422 (1981).
[23] E.-J. Cho, S.-J. Oh, S. Suga, T. Suzuki, and T. Kasuya, J. Electron Spectrosc., **77**, 173 (1996).
[24] Y. Ohno and T. Urata, J. Electron Spectrosc., **125**, 171 (2002).
[25] B. A. Orlowski, S. Mickevicius, M. Chernyshova, I. Demchenko, A. Y. Sipatov, T. Story, V. Medicherla, and W. Drube, J. Electron Spectrosc., **137**–**140**, 763 (2004).
[26] B. A. Orlowski, S. Mickievicius, V. Osinniy, A. J. Nadolny, B. Taliashvili, P. Dziawa, T. Story, R. Medicherla, and W. Drube, Nucl. Instrum. Meth. B, **238**, 346 (2005).
[27] K. H. J. Buschow, M. Campagna, and G. K. Wertheim, Solid State Commun., **24**, 253 (1977).
[28] E.-J. Cho, S.-J. Oh, S. Imada, S. Suga, T. Suzuki, and T. Kasuya, Phys. Rev. B, **51**, 10146 (1995).
[29] S. Miyazaki, J. Vac. Sci. B, **19**, 2212 (2001).
[30] E.-J. Cho and S.-J. Oh, Phys. Rev. B, **59**, R15613 (1999).
[31] F. Mercier, C. Alliot, L. Bion, N. Thromat, and P. Toulhoat, J. Electron Spectrosc., **150**, 21 (2006).
[32] R. Vercaemst, D. Poelman, L. Fiermans, R. L. Van Meirhaeghe, W. H. Laflère, and F. Cardon, J. Electron Spectrosc., **74**, 45 (1995).
[33] A. Kotani and H. Ogasawara, J. Electron Spectrosc., **60**, 257 (1992).
[34] Scientific Group Thermodata Europe: The Landolt-Börnstein Database, *Thermodynamic Properties of Inorganic Materials*, Vol. 19A1 (Springer Materials, 2000) ISBN 978-3-540-64734-8.
[35] T. Hattori, K. Azuma, Y. Nakata, M. Shioji, T. Shiraishi, T. Yoshida, K. Takahashi, H. Nohira, Y. Takata, S. Shin, and K. Kobayashi, Appl. Surf. Sci., **234**, 197 (2004), ISSN 0169-4332.